Dynamic MRI Visualization of Two-Phase Flow in a Ceramic Monolith

M. D. Mantle, A. J. Sederman, and L. F. Gladden
Dept. of Chemical Engineering, University of Cambridge, Cambridge CB2 3RA, U.K.

S. Raymahasay and J. M. Winterbottom
School of Chemical Engineering, University of Birmingham, Edgbaston, Birmingham B15 2TT, U.K.

E. H. Stitt
Synetix, Billingham, Cleveland TS23 1LB, U.K.

Regular and irregular catalyst packings are extensively used in the chemical industry for promoting mass transfer and chemical reaction between gas and liquid. Traditionally, randomly packed beds of catalyst particles operating in co-current downflow operation, often termed trickle-bed reactors, have been used because of the high mass-transfer rates achievable. More recently, structured supports are increasingly considered for use because of the potential improvements they offer with respect to, for example, the decoupling of heat- and mass-transfer phenomena, operation under reduced pressure drop conditions and at much higher gas/liquid flow rates, and a greater resistance to attrition (Irandoust and Andersson, 1988a,b; Irandoust et al., 1998; Kapteijn et al., 1999). Monoliths, which comprise a metal or ceramic structure with a large number of straight or parallel channels, are an example of such structured supports, and their use in solid-catalyzed gas-phase chemical reactions is well established. One example is the monolithic exhaust converter used throughout the automotive industry. In contrast, the application of monoliths to gas-liquid reactions is not well advanced and a significant research activity exists to provide the necessary understanding to enable reliable scale-up for process operation (Nijhuis et al., 2001). Undoubtedly, such efforts would be significantly aided if it were possible to develop an *in-situ* probe of the multiphase transport and reaction phenomena occurring within these porous structures. Magnetic resonance techniques show particular promise in this regard because of their ability to provide chemically-specific information on both the internal phase distribution and transport processes occurring within three-dimensional (3-D) optically opaque systems.

Visualization of gas-liquid flow in ceramic monoliths has previously been attempted by Mewes et al. (1999) using the capacitance tomography technique. While temporal resolution of capacitance tomography is high (100 images per second can be achieved), spatial resolution is relatively low with typical in-plane resolutions being 5–10% of the diameter of the system under investigation, thereby making impossible visualization of phase distribution within a single channel. In contrast, magnetic resonance imaging (MRI) has the potential for relatively high spatial resolution (say, 30–200 μm), but the temporal resolution obtained for gas-liquid flow has to date been far too slow to visualize dynamic processes occurring in reactors. Time-averaged visualizations of single- and two-phase flow have been reported with data acquisition times of minutes to hours (Sederman et al., 1998; Tallarek et al. 1998; Johns et al., 2000; Sederman and Gladden, 2001; Mantle et al., 2001). Fast velocity imaging techniques have been reported which are able to acquire liquid velocity images in several minutes (Seifert et al., 2000; Scheenen et al., 2000), but these techniques can only be applied to systems characterized by low fluid velocities and where the flow fields are temporally steady. Koptyug et al. (2000) have also used MRI to obtain velocity images of single-phase steady-state gas flow through a monolith catalyst support. Typical image acquisition times are 20 to 40 min.

The purpose of this article is to report the development and application of a novel MRI technique which provides 2-D images of in-plane resolution 391 μm $\times$ 781 μm, with a data acquisition time of 160 ms. The technique is robust in application to systems characterized by significant magnetic susceptibility variations and rapid nuclear spin relaxation times. These characteristics are typical of the multiphase systems of interest in chemical engineering, and, therefore, this technique provides a first opportunity to study nonsteady-state phase distribution in optically opaque environments under a range of conditions configured within the imaging volume. Possible applications are the distribution of two phases during displacement processes in rock cores, moisture migration during drying within particle arrays, and time-resolved visual-

Correspondence concerning this article should be addressed to L. F. Gladden.

ization of phase distribution within multiphase flows in packed-bed reactors. Limitations on the spatial resolution obtained will depend on the magnetic resonance characteristics of the system being studied. The system considered here represents one of the more challenging systems to visualize due to the high magnetic susceptibility variations present; hence, the resolution reported here should be readily achieved in any (nonferromagnetic) system of interest to chemical engineers. In this article, the capabilities of this technique are illustrated with application to gas-liquid flow (more commonly referred to as Taylor flow or bubble-train flow) through a ceramic square-channel monolith system, for which it is demonstrated that bubble-size distributions, phase volume fractions, and bubble-velocity distributions can be obtained. The technique is entirely general and can therefore be applied to obtain rapid, time-resolved visualization of phase distribution within many gas-liquid-solid systems.

Experimental Methods

Flow Cell

A glass column (48 mm I.D.) containing a cylindrical square-channel monolith was positioned within the vertical bore of the magnet. The ceramic (cordierite) monolith of 43 mm dia. and 0.15 m length was rated at 400 channels per square in. with each channel having a square cross-section of 1.2 mm side. Gas (compressed air) and liquid (water) were introduced at the top of the column as two separate feedstreams with flow rates of 1 L min^{-1} and 6 L min^{-1}, respectively. The superficial flow direction was along the axis of the magnet, that is, in the z-direction. The high velocity liquid jet at the column inlet created an intensely agitated gas-liquid dispersion (Boyes et al., 1992) flowing downwards and the upper surface of the monolith was positioned at a distance 0.85 m below the inlet. The column was operated under recycled cocurrent downflow conditions with a pressure drop of 0.0024 barg across the monolith, not including the hydrostatic head.

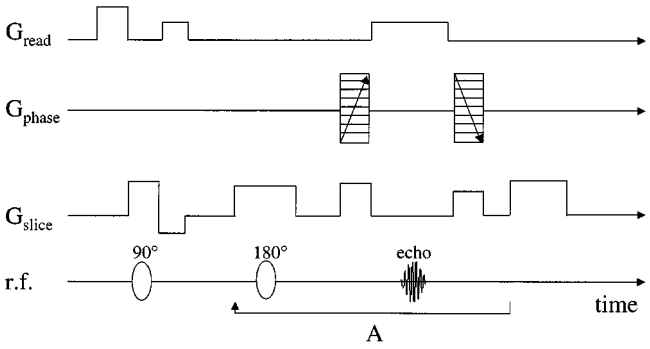

Figure 1. Single-shot 2-D RARE r.f. pulse sequence used.

The loop A of successive 180° radio-frequency (rf) refocusing pulses is repeated 256 times enabling rapid acquisition of the 2-D data for a single initial 90° rf excitation. The rf pulses and magnetic field gradients are: 90° soft excitation pulse = 500 μs Gaussian truncated at 5%; read gradient = 12.0 Gcm^{-1}; phase gradient = 6.39 Gcm^{-1}; slice gradient = 5.84 Gcm^{-1}. The 180° rf pulse after every read gradient allows the read direction to be the same for all lines of k-space, thus avoiding odd/even echo ghosting artifacts.

MRI

MRI experiments were carried out on a Bruker Spectrospin DMX 200, 4.7 T magnet with a birdcage coil of 6.3 cm length and diameter. Proton (^{1}H) images were acquired at a frequency of 199.7 MHz. Spatial resolution was achieved using shielded gradient coils providing a maximum gradient strength of 13.90 G cm^{-1}. The effective spin-spin relaxation time T_2^* of the water within the monolith was 1 ms. Figure 1 shows the pulse sequence used to obtain 2-D images in the xz plane. The pulse sequence is based on the 2-D "Single Shot RARE" (or Turbo Spin Echo) pulse sequence (Hennig et al., 1986); in this experiment a single 2-D image is acquired for each excitation pulse, and successive images can be acquired at time intervals of a few seconds. In the present work, this

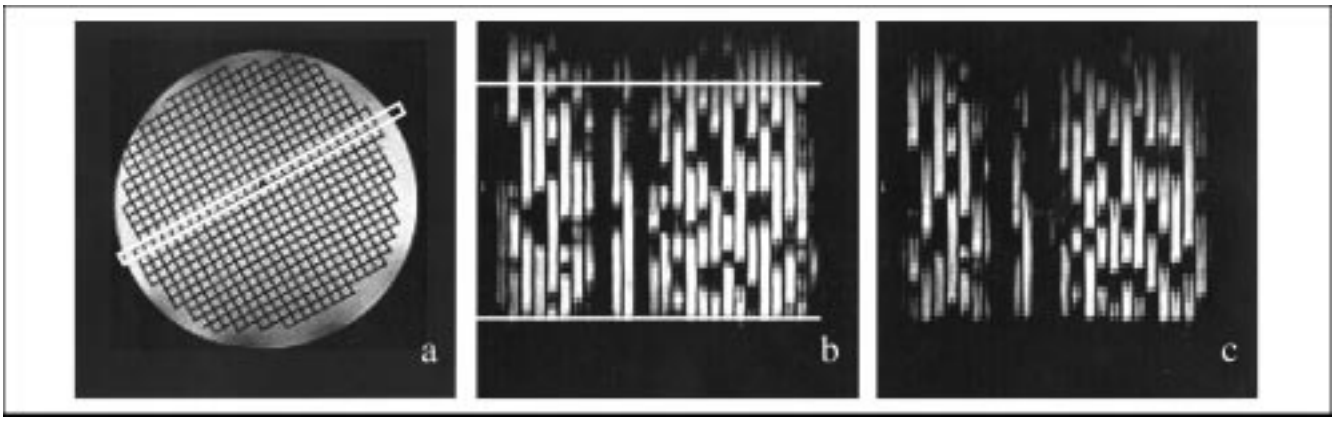

Figure 2. ^{1}H magnetic resonance visualizations within the ceramic monolith.

Xy-image of the fully water-saturated monolith (a) monolith's internal structure; each channel has a side length 1.2 mm. It highlights the image slice position in the xz direction for which the visualizations of gas-liquid distribution during two-phase flow are shown (b and c). Data acquisition time for each image was 160 ms; there was a time period of 160 ms between the start of each of the images shown in (b) and (c). In all images, the presence of water is indicated by high intensity (white); gas and ceramic are identified by zero intensity (black). The area within the solid white bars in (b) defines the analysis region.

pulse sequence is modified such that a single excitation is used to acquire a number of images (four in this case) in immediate succession; the details of the implementation of this new pulse sequence will be published elsewhere (Sederman et al., 2001). Each image took 160 ms to acquire and the time between the start of successive acquisitions was also 160 ms. Therefore, effective image times are taken as 80, 240, 400 and 560 ms after the initial excitation. Subsequent sets of four images were acquired following a time delay of 3 s; this delay could be reduced to less than 1 s with suitable gradient cooling. Figure 2a shows a 2-D transverse (xy) ^{1}H image of a fully water-saturated monolith in the absence of flow; in-plane spatial resolution is 391 μm $\times$ 391 μm. The boxed area shows the location of the xz slice for which visualizations are shown in Figures 2b and 2c. The visualizations in Figures 2b and 2c consist of a 128 (x-read) $\times$ 64 (z-phase) data array with a field-of-view of 50 mm $\times$ 50 mm, which yields an in-plane pixel resolution of 391 μm $\times$ 781 μm. The imaging section was chosen to focus on the monolith outlet. The thickness of the image slice is 1.0 mm. Following acquisition, the data were transferred to a Sun Sparc 20 workstation for processing using in-house software.

Results and Discussion

Inspection of Figures 2b and 2c clearly shows it is possible to visualize individual gas bubbles (zero image intensity) within the channels of the monolith. Liquid films on the walls of the monolith were not observed, although, in principle, it might be possible to optimize the magnetic resonance experiment to address the characterization of such films; the typical film thickness is expected to lie in the range 5–50 μm (Thulasidas et al., 1995). Bubble-size and velocity distributions are obtained by binary gating each image as shown in Figure 3a, such that each image pixel is identified as containing either gas (black), liquid (white), or solid monolith (grey). The value at which the image pixel intensities are gated is obtained by plotting a histogram of image intensities, characterized by two peaks corresponding to pixels filled with gas (or ceramic) or liquid; the gating level is identified as the pixel intensity which is positioned at the midpoint in the intensity distribution between these two peaks. Figure 3b shows the bubble-size distribution directly obtained from the gated image shown in Figure 3a. The liquid-phase volume fraction obtained from Figure 3a is 0.61 ± 0.03 which compares well with values volumetrically obtained for liquid holdups in normal cocurrent downflow contactor reactor operation, typically 0.5–0.7 (Boyes et al., 1992). The error estimate takes into account the sensitivity of the result to both (a) a 10% shift in the image intensity selected as the gating level, and (b) finite pixel effects which occur when, for example, a given pixel containing some gas or ceramic is assigned as totally liquid-containing, as a result of the image-analysis procedure. It is noted that the implementation of this RARE-based technique provides a measurement which is particularly robust with respect to motion in the phase encoding direction, that is, the technique is relatively insensitive to flow artifacts. This insensitivity to velocity artifacts arises because there is not only a phase unwind gradient (hence, the phase gradients act as small velocity encoding gradients), but the following phase wind/unwind gradient pair (although having a slightly reduced magnitude due to them encoding a different part of k_y-space) act as velocity-compensating gradients, thereby minimizing the effect of velocity artifacts in the measurements. Errors in bubble size and velocity as a result of 'blurring' in the image arising from the translational motion of the bubble between each successive phase winding gradient are considered negligible; a detailed analysis of this has been considered elsewhere (Sederman et al., 2001). In summary, blurring is seen as a monotonic decrease in signal intensity in the region of the gas-liquid interface defining the boundary of the bubble. We define the "image time" associated with each image as the mid-point in the overall acquisition time for that image; given that, we position the binary gate at the mid-point in the observed signal intensity. This positioning of the gas-liquid interface in our data analysis procedure identifies the position of the interface at the "image time." Images acquired over data acquisition times of 100 ms yield the same bubble-size and velocity distributions as those reported here.

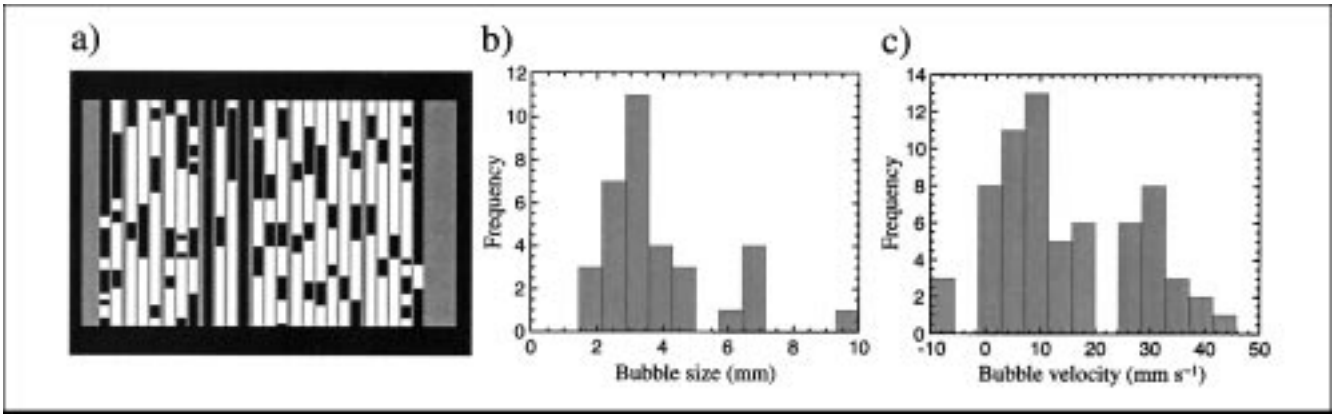

Figure 3. Obtaining bubble-size and bubble-velocity distributions.

Images are first binary gated: (a) image in Figure 2b after binary gating. The bubble-size distribution is obtained directly from this gated image. The distribution of bubble velocities is obtained by identifying the position of the gas-liquid interface in two successive visualizations recorded for a single rf excitation. Apparent varying wall thickness between channels results from the image analysis process in which pixels are associated with only one phase gas, liquid, or ceramic. The upper error limit in determining bubble size and velocity is 20%.

The bubble-velocity distribution shown in Figure 3c is obtained by following the position of the gas-liquid interface characterizing each bubble between successive pairs of images, in this case the images shown in Figures 2b and 2c. It should be noted that only bubbles wholly contained within the area bounded by white lines in Figure 2b are included in the analysis. Analysis of the data presented here confirm that the system is demonstrating bubble-train flow and that MRI can be used as a quantitative tool to probe two-phase flow within ceramic channels over very short (that is, 160 ms) time-scales. Preliminary observations which can be directly made from a sequence of four images are:

(a) In the case when more than one gas bubble exists within the same channel, the velocity of each bubble, as calculated using two successively acquired images, is the same.

(b) Throughout the sequence of four images, a given bubble does not change in size to within the spatial resolution of the experiment (bubble-length changes of greater than 781 μm would be detected).

(c) Using the four images (1–4) acquired following a given r.f. excitation, it is possible to calculate bubble velocity as a function of time by comparing bubble displacement between (a) images 1 and 2; (b) images 2 and 3; (c) images 3 and 4. This analysis shows that the bubble velocity is not stable with time.

(d) Bubble motion in the direction opposite to that of the superficial flow is observed in one channel as expected given the possibility of negative pressure drop existing at different locations across the monolith (Mewes et al., 1999).

(e) No correlation was observed between bubble size and bubble velocity.

The development in MRI technique implemented here demonstrates that MRI can now be applied to look at dynamic processes in the highly magnetically heterogeneous environments characteristic of many systems encountered in chemical engineering. Future work will use this rapid data acquisition methodology to study chemically reactive systems where we will also exploit the chemical-specific nature of magnetic resonance measurements.

Acknowledgments

We gratefully acknowledge financial support for this work from Johnson Matthey plc, Synetix, Chart Heat Exchangers Ltd., Robinson Brothers Ltd., Thomas Swan & Co. Ltd., Quest International (Fragrances) U.K. Ltd., and DTI LINK. We also wish to thank Johnson Matthey plc for provision of the ceramic monolith.

Literature Cited

Boyes, A. P., A. Chughtai, X. X. Lu, S. Raymahasay, S. Sarmento, M. W. Tilston, and J. M. Winterbottom, "The Cocurrent Downflow Contactor (CDC) Reactor - Chemically Enhanced Mass-Transfer and Reaction Studies for Slurry and Fixed-Bed Catalytic-Hydrogenation," *Chem. Eng. Sci.*, **47**, 3729 (1992).

Hennig, J., A. Nauerth, and H. Friedburg "Rare Imaging - a Fast Imaging Method for Clinical MR," *Mag. Res. Med.*, **3**, 823 (1986).

Irandoust, S., and B. Andersson "Monolithic Catalysts for Non-automobile Applications," *Catal. Rev. Sci. Eng.*, **30**, 341 (1988a).

Irandoust, S., and B. Andersson "Mass Transfer and Liquid-Phase Reactions in a Segmented Two-Phase Flow Monolithic Catalytic Reactor," *Chem. Eng. Sci.*, **43**, 1983 (1988b).

Irandoust, S., A. Cybulski and J. A. Moulijn, "The Use of Monolithic Catalysts for Three Phase Reaction," *Structured Catalysts and Reactors*, A. Cybulski and J. A. Moulijn (eds.), Marcel Dekker, New York, p. 239 (1998).

Johns, M. L., A. J. Sederman, A. S. Bramley, L. F. Gladden, and P. Alexander, "Local Transitions in Flow Phenomena Through Packed Beds Identified by MRI," *AIChE J.*, **46**, 2151 (2000).

Kapteijn, F., J. J. Heiszwolf, T. A. Nijhuis, and J. A. Moulijn, "Monoliths in Multiphase Catalytic Processes," *CatTech*, **5**, 24 (1999).

Koptyug, I. V., S. A. Altobelli, E. Fukushima, A. V. Matveev, and R. Z. Sagdeev, "Thermally Polarized H-1 NMR Microimaging Studies of Liquid and Gas Flow in Monolithic Catalysts," *J. Mag. Res.*, **147**, 36 (2000).

Mantle, M. D., A. J. Sederman, and L. F. Gladden, "Single- and Two-Phase Flow in Fixed-Bed Reactors: MRI Flow Visualisation and Lattice-Boltzmann Simulations," *Chem. Eng. Sci.*, **56**, 523 (2001).

Mewes, D., T. Loser, and M. Millies, "Modelling of Two-phase Flow in Packings and Monoliths," *Chem. Eng. Sci.*, **54**, 4729 (1999).

Nijhuis, T. A., M. T. Kreutzer, A. C. J. Romijn, F. Kapteijn, and J.A. Moulijn, "Monolithic Catalysts as Efficient Three-Phase Reactors," *Chem. Eng. Sci.* **56**, 823 (2001).

Scheenen, T. W. J., D. van Dusschoten, P. A. de Jager, and H. van As, "Microscopic Displacement Imaging with Pulsed Field Gradient Turbo Spin-Echo NMR," *J. Mag. Res.*, **142**, 207 (2000).

Sederman, A. J., M. L. Johns, P. Alexander, and L. F. Gladden, "Structure-flow Correlations in Packed Beds," *Chem. Eng. Sci.*, **53**, 2117 (1998).

Sederman, A. J., and L. F. Gladden, "Magnetic Resonance Imaging as a Quantitative Probe of Gas-Liquid Distribution and Wetting Efficiency in Trickle-Bed Reactors," *Chem. Eng. Sci.*, **56**, 2615 (2001).

Sederman, A. J., M. D. Mantle, and L. F. Gladden, "Non-Steady State Two-Phase Flow Velocity Imaging Using Single Excitation Multiple Image Acquisition," submitted to *J. Mag. Res.* (2001).

Seifert, M. H. J., P. M. Jakob, V. Jellus, A. Haase, and C. Hillenbrand, "High-resolution Diffusion Imaging Using a Radial Turbo-Spin- Echo Sequence: Implementation, Eddy Current Compensation, and Self-navigation," *J. Mag. Res.*, **144**, 243 (2000).

Tallarek, U., E. Bayer, D. van Dusschoten, T. Scheenen, H. van As, G. Guiochon, and U. D. Neue, "Dynamic NMR Microscopy of Chromatographic Columns," *AIChE J.*, **44**, 1962 (1998).

Thulasidas, T. C., M. A. Abraham and R. L. Cerro "Bubble-Train Flow in Capillaries of Circular and Square Cross Section," *Chem. Eng. Sci.*, **50**, 183 (1995).

Manuscript received May 10, 2001, and revision received Oct. 23, 2001.